IEEE Photonics Journal
An IEEE Photonics Society Publication

Open Access

95.16-Gb/s Mode-Division-Multiplexing Signal Transmission in Free-Space Enabled by Effective-Conversion of Vector Beams

Volume 9, Number 4, August 2017

Jianbo Zhang
Fan Li
Jianping Li, ***Member, IEEE***
Zhaohui Li

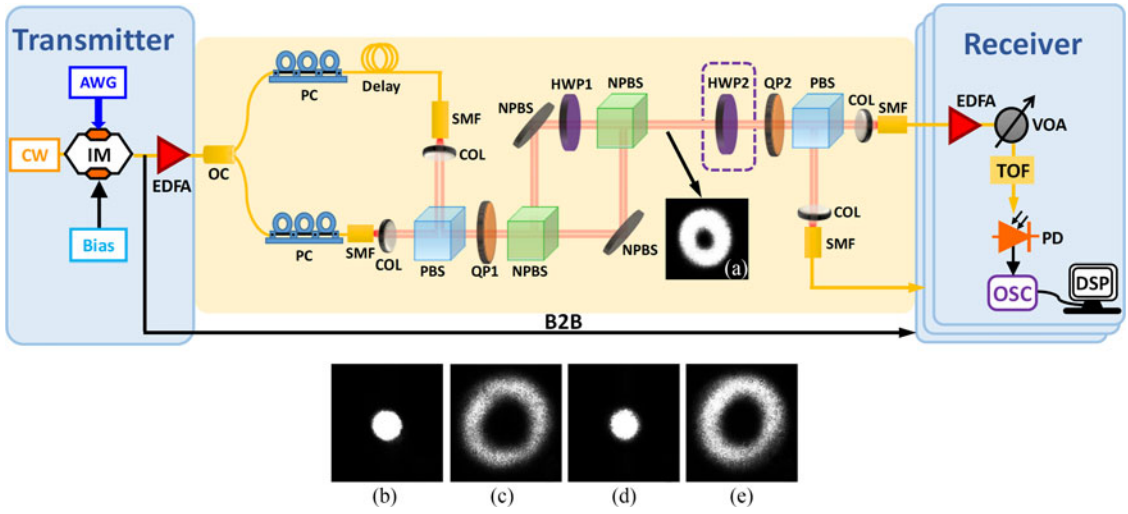

DOI: 10.1109/JPHOT.2017.2713803
1943-0655 © 2017 IEEE

95.16-Gb/s Mode-Division-Multiplexing Signal Transmission in Free-Space Enabled by Effective-Conversion of Vector Beams

Jianbo Zhang,[1] Fan Li,[2] Jianping Li,[1] *Member, IEEE*, and Zhaohui Li[2]

[1]Guangdong Provincial Key Laboratory of Optical Fiber Sensing and Communications, Institute of Photonics Technology, Jinan University, Guangzhou 510632, China
[2]State Key Laboratory of Optoelectronic Materials and Technologies, School of Electronics and Information Technology, Sun Yat-Sen University, Guangzhou 510275, China

DOI:10.1109/JPHOT.2017.2713803

Manuscript received April 22, 2017; revised June 2, 2017; accepted June 6, 2017. Date of publication June 8, 2017; date of current version June 19, 2017. This work was supported in part by the National High Technology 863 Research and Development of China under Grant 2015AA017102, in part by the National Science Foundation of China under Grants 61575082, 61601199, 61525502, and 61435006, in part by the Youth Science and Technology Innovation Talents of Guangdong under Grant 2015TQ01X606, in part by the Guangdong Provincial Natural Science Foundation under Grant 2015A030313328, in part by the Pearl River S&T Nova Program of Guangzhou under Grant 201710010051, in part by the Fundamental Research Funds for the Central Universities under Grant 21615450. Corresponding author: Jianping Li (e-mail: jpli@live.cn).

Abstract: We introduce a high-efficient vector modes (VMs) conversion scheme by using Q-plate (QP) and half-waveplate based on higher-order Poincaré sphere model. Enabled by this simple mode conversion scheme, we demonstrate a 95.16-Gb/s vector-mode-division-multiplexing (VMDM) transmission with direct-detection orthogonal-frequency-division-multiplexing signal over ∼20-cm free space optical link. The mode crosstalk of four typical cylindrical VMs (TE01, TM01, HE21e, and HE21o) are less than −10.3 dB and can be further optimized by high-quality QP. The experimental results indicate that the VMDM technique can be a powerful candidate for large-capacity short-reach optical interconnects.

Index Terms: Fiber optics and optical communications, vector mode, mode-division-multiplexing (MDM), direct detection orthogonal frequency division multiplexing (DD-OFDM), optical interconnect, polarization.

1. Introduction

The developments of bandwidth-hungry services in data center or super-computing center are leading to data explosion [1], so the capability of short-reach optical interconnection systems should be urgently improved to meet the ever-growing demand for data traffic. To break through the capacity bottleneck, multi-dimensional multiplexing techniques of optical signal in the domain of time, frequency, polarization and phase have been studied and applied to commercial systems successfully. However, since the low cost and power consumption are the most important concern for the short reach optical interconnection systems, traditional wavelength division multiplexing, polarization multiplexing techniques and coherent detection technique cannot be used in data center or super-computing center [2]. To relieve bandwidth requirements and satisfy ultra-high

capacity, mode division multiplexing (MDM) technique has been proposed to deal with this challenge [3]. Due to their orthogonality, different spatial modes at the same wavelength can be treated as parallel and independent channels to achieve large-capacity transmission systems only based on low-cost and low power consumption direct detection (DD) technologies [4]–[6]. Thus, the MDM-DD-based scheme in short-reach optical interconnects shows its potential in terms of cost, complexity and power consumption [7], [8]. Recently, MDM communication systems have been successfully demonstrated based on linearly polarized mode (LPM) [6]–[8], orbital angular momentum (OAM) [9]–[13], Laguerre–Gaussian mode [14] and Bessel modes [15].

Vector mode (VM) is also introduced lately as a new orthogonal multiplexing technique due to its good performance [16]–[19]. First, the VMs are the eigen modes of the full vector electromagnetic wave equation with spatially variant states of polarization (SOP) in fiber, and can be generally referred to cylindrical vector beams (CVBs) if the SOP is cylindrical symmetry [20]. Researchers have demonstrated that these beams can be generated and propagated in optical fibers with good performance [21]. So, it will demonstrate a stable transmission characteristic in fiber transmission. In addition, it has been demonstrated that CVBs are less susceptible to atmospheric turbulence, which indicates that they are also useful and promising in free space optical (FSO) communication [22].

Many schemes have been implemented to generate VM, such as laser intracavity devices [23], special optical fibers [21], liquid crystal technology [24], [25], and metasurface [26] etc. All these VMs generating components can be classified as mode converters which are the key components to realize the VM-based MDM transmission systems [27]. It is important to use simple and cost-effective optical components to achieve arbitrary higher-order VM generation. The arbitrary order VMs can be obtained simply by combing a few Q-plate (QPs) and half-wave plates (HWPs) or quarter-wave plates (QWPs) [28], [29].

In the previous work [17], the 4 $\times$ 20 Gb/s vector-MDM (VMDM) transmission over $\sim$1 m FSO link has been demonstrated by using 4 QPs with higher mode isolation with coherent detection. Although the data rate is relatively high, as coherent detection is applied in that scheme, it is not suitable for optical interconnect due to its high cost. Meanwhile, we have also demonstrated the high-speed 2 $\times$ 60 Gb/s VMDM-based transmission over $\sim$80 cm FSO link by using 2 QPs with relative lower mode isolation with direct detection [19]. Due to the used vector modes with the feature of CVB, the demonstrated experiments can be recognized as the CVB-based VMDM transmission systems. In order to further relieve bandwidth requirement, more VMs are required to be used to transmit signal.

In this paper, we introduce the higher-order Poincaré sphere model to obtain the higher-order CVBs conversion with QPs and HWPs. Then, we apply this flexible mode conversion scheme to implement the high-speed CVB-based VMDM short-reach optical inter-connection system. A 95.16 Gb/s 4-CVB VMDM-DD-OFDM transmission has been successfully demonstrated over $\sim$20 cm FSO link without multiple-input multiple-output (MIMO) digital signal processing (DSP). This demonstration is different with previous works since only 2 QPs are used to generate the 4 CVBs and the mode crosstalk is higher among them. The results show that the proposed method can be a good candidate for large-capacity VMDM based short-reach optical interconnects, such as the board-to-board or rack-to-rack interconnect in data center or super-computing center.

2. Concept and Principle

Theoretically, vector modes are the solutions to the Maxwell's equation in vector form. The SOP of VMs can be described as Jones vector [30],

$$|l, \gamma\rangle = \left[\cos(l\varphi + \gamma)\ \sin(l\varphi + \gamma)\right]^{\mathrm{T}} \tag{1}$$

Where l is the order of VMs ($l = \pm 1, \pm 2, \ldots$) and γ is the initial polarization rotation of VMs ($\gamma = 0, \pi/2$). The φ represents the azimuth on the transverse plane. In this description, each vector mode is axial symmetry in polarization distribution pattern and can be characterized by l and γ.

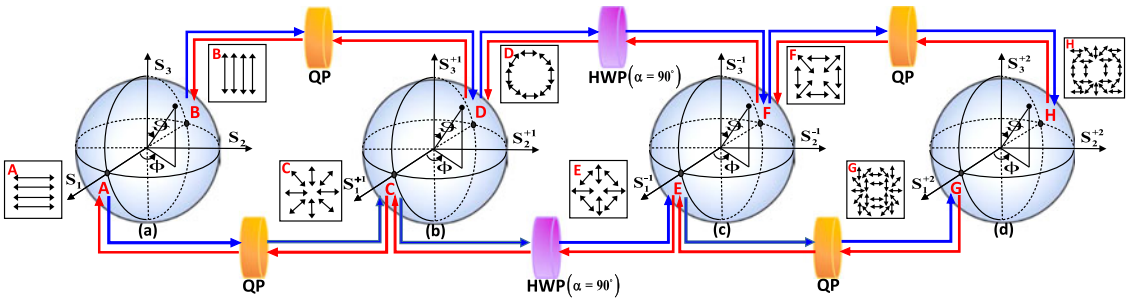

Fig. 1. (a) The fundamental Poincaré sphere ($l = 0$) indicates the uniform polarization of a light beam. (b), (c) and (d) represent the polarization for l = 1, l = −1 and l = 2 on the higher-order Poincaré sphere, respectively.

Fig. 1 illustrates the transformation of vector beams based on the higher-order Poincaré spheres proposed in [31]. θ and ϕ are the colatitude and azimuth angles over the sphere ($\theta \in [0, \pi]$, $\phi \in [0, 2\pi]$). Then, an arbitrary SOP $\psi_l(\theta, \phi)$, which is mapped by a point on a unit sphere, can be described as follows,

$$\Psi_l|\theta, \phi\rangle = \cos\left(\frac{\theta}{2}\right)|L_l\rangle\, e^{\frac{i\phi}{2}} + \sin\left(\frac{\theta}{2}\right)|R_l\rangle\, e^{-\frac{i\phi}{2}} \tag{2}$$

Where $|L_l\rangle = (\hat{x} + i\hat{y})e^{-il\varphi}/\sqrt{2}$ and $|R_l\rangle = (\hat{x} - i\hat{y})e^{il\varphi}/\sqrt{2}$ are left and right-circular polarizations corresponding to north and south poles on the sphere, respectively. l is the order of Poincaré spheres and φ is the azimuthal angle. The point of equators in Fig. 1.(b)–(d) correspond to inhomogeneous linear polarization. The polarization of other points except for those located at poles and equators correspond to elliptical polarization. Then the SOP of the point located at the equator of higher-order Poincaré sphere can be expressed by the Jones vector,

$$\Psi_l\left|\frac{\pi}{2}, \phi\right\rangle = \left[\cos\left(\tfrac{\phi}{2} - l\varphi\right) - \sin\left(\tfrac{\phi}{2} - l\varphi\right)\right]^{\mathrm{T}} \tag{3}$$

As we can find from Fig. 1(b) that the points of C $(\cos\varphi \sin\varphi)^T$ and D $(\sin\varphi - \cos\varphi)^T$ are radial and azimuthal polarization CV beams, respectively. Apart from C and D, the other points of the equator are generalized CV beams as a linear superposition of C and D. As one kind of vector mode converter, the QP that has a special topological charge of q can be used to convert the homogenous linear polarized beams to the desired VMs. QP is a passive liquid crystal optical element whose retardation can be controlled by a direct-current bias. The Jones matrix of QP can be expressed as [32],

$$J_s = \begin{bmatrix} \cos 2(q\varphi + \alpha_0) & \sin 2(q\varphi + \alpha_0) \\ \sin 2(q\varphi + \alpha_0) & -\cos 2(q\varphi + \alpha_0) \end{bmatrix} \tag{4}$$

Where q of the used QP equals 1/2. α_0 is a constant offset angle which represents the initial polarization direction for $\varphi = 0$. In general, the QP or other VM converter is enough to realize the desired VM conversion if we need not to consider the availability of experimental components. However, it is important to achieve more efficient and flexible VMs conversion only with limited experimental resources, such as lack of the required QPs. Fortunately, the HWP is a common optical component and usually used to modify the polarization state of light beams. Thus, we can apply this feature of HWP to implement the desired CVBs effectively with available QPs. The transfer function of a HWP with fast axis at angle α can be represented as follows,

$$P = \begin{bmatrix} \cos\alpha & -\sin\alpha \\ \sin\alpha & \cos\alpha \end{bmatrix} \begin{bmatrix} \exp(i\pi/2) & 0 \\ 0 & \exp(i\pi/2) \end{bmatrix} \begin{bmatrix} \cos\alpha & \sin\alpha \\ -\sin\alpha & \cos\alpha \end{bmatrix} \tag{5}$$

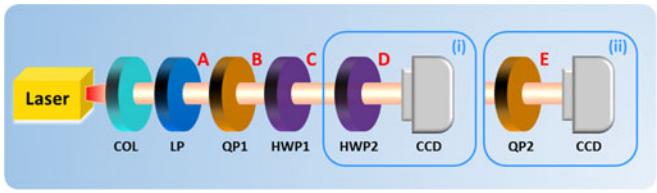

Fig. 2. Experimental setup to validate the effective VMs conversion and transformation between different SOPs. COL: collimator; LP: linear polarizer; QP: Q-plate; HWP: half-wave plate; CCD: charged-coupled device camera.

Then the resulting transformation can be expressed as follows (supposing $\alpha_0 = 0$),

$$\Psi_0 \left|\frac{\pi}{2}, \phi\right\rangle \overset{\text{QP}}{\leftrightarrows} \Psi_1 \left|\frac{\pi}{2}, -\phi\right\rangle \tag{6}$$

$$\Psi_1 \left|\frac{\pi}{2}, \phi\right\rangle \overset{\text{HWP}}{\leftrightarrows} \Psi_{-1} \left|\frac{\pi}{2}, -(\phi + 4\alpha)\right\rangle \tag{7}$$

$$\Psi_{-1} \left|\frac{\pi}{2}, \phi\right\rangle \overset{\text{QP}}{\leftrightarrows} \Psi_2 \left|\frac{\pi}{2}, -\phi\right\rangle \tag{8}$$

As we can see, the polarization state of beam located at the equator of a sphere can be transferred to another sphere using QP or HWP. Take the marked points (A, C, E, and G in Fig. 1) as an example, the basic SOP conversion can be simply understood as follows,

$$\underbrace{(1, 0)^{\mathrm{T}}}_{\text{Apoint}} \overset{\text{QP}(\alpha_0=0)}{\leftrightarrows} \underbrace{(\cos\varphi, \sin\varphi)^{\mathrm{T}}}_{\text{Cpoint}} \overset{\text{HWP}(\alpha=\pi/2)}{\leftrightarrows} \underbrace{(\cos\varphi, -\sin\varphi)^{\mathrm{T}}}_{\text{Epoint}} \overset{\text{QP}(\alpha_0=0)}{\leftrightarrows} \underbrace{(\cos 2\varphi, \sin 2\varphi)^{\mathrm{T}}}_{\text{Gpoint}} \tag{9}$$

Moreover, this analysis can be generally summarized as,

$$\Psi_l \left|\frac{\pi}{2}, \phi\right\rangle \overset{\text{QP}(\alpha_0=0)}{\leftrightarrows} \Psi_{(2q-l)} \left|\frac{\pi}{2}, -\phi\right\rangle \tag{10}$$

$$\Psi_l \left|\frac{\pi}{2}, \phi\right\rangle \overset{\text{HWP}}{\leftrightarrows} \Psi_{-l} \left|\frac{\pi}{2}, -(\phi + 4\alpha)\right\rangle \tag{11}$$

From the above formulas, the relationship of different order vector modes based on QP and HWP can be easily established. This analysis can be further expanded to arbitrary order VMs by applying more QPs and HWPs.

3. Experimental Results and Discussion

3.1. Verification of VM Generation

The experimental setup of the CV mode conversion is shown in Fig. 2. The laser source ($\lambda = 1550$ nm, 12.5 dBm) is collimated (COL) to a beam with waist of ~2.1 mm and transformed to a homogeneous linearly polarized beam via linear polarizer (LP). Then, we use an electrically driven QP (QP1) to generate the desired CVBs. The Q-plate in experiment is the one produced by Arcoptix [33] with $q = 1/2$. Fig. 3 $(A_1)/(A_2) \sim (E_1)/(E_2)$ show the intensity patterns captured by the charged-coupled device (CCD) camera at the labelled points (A, B, C, D and E) in Fig. 2. As we can see from Fig. 3, the transmitted beams are transformed to the doughnut shaped beams after passing through QP1. Namely, the horizontal /vertical linear polarized beams are converted to TM_{01} /TE_{01} modes by QP1. After passing through HWP1 with fast axis at $\pi/2$, TM_{01}/TE_{01} modes are transformed into $HE_{21}^{\text{even}}/HE_{21}^{\text{odd}}$ modes. The Inset 2(i) in Fig. 2 is employed to illustrate the inverse process of (7). $HE_{21}^{\text{even}}/HE_{21}^{\text{odd}}$ modes can be also converted to TM_{01} /TE_{01} modes by HWP2. If we replace HWP2 with QP2 (inset 2(ii)), $HE_{21}^{\text{even}}/HE_{21}^{\text{odd}}$ modes are transformed to higher-order VMs. Fig. 3 $(b_1)/(b_2) \sim (e_1)/(e_2)$ depict

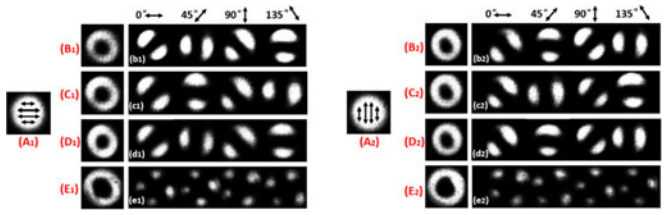

Fig. 3. Insets $(A_1)/(A_2)$ ~$(E_1)/(E_2)$ depict the intensity profiles of labelled points in Fig. 2 captured by CCD camera. The arrows indicate the orientations of the transmission axis of the LP. Insets $(b_1)/(b_2)$ ~$(e_1)/(e_2)$ show the polarization distribution of the corresponding VMs.

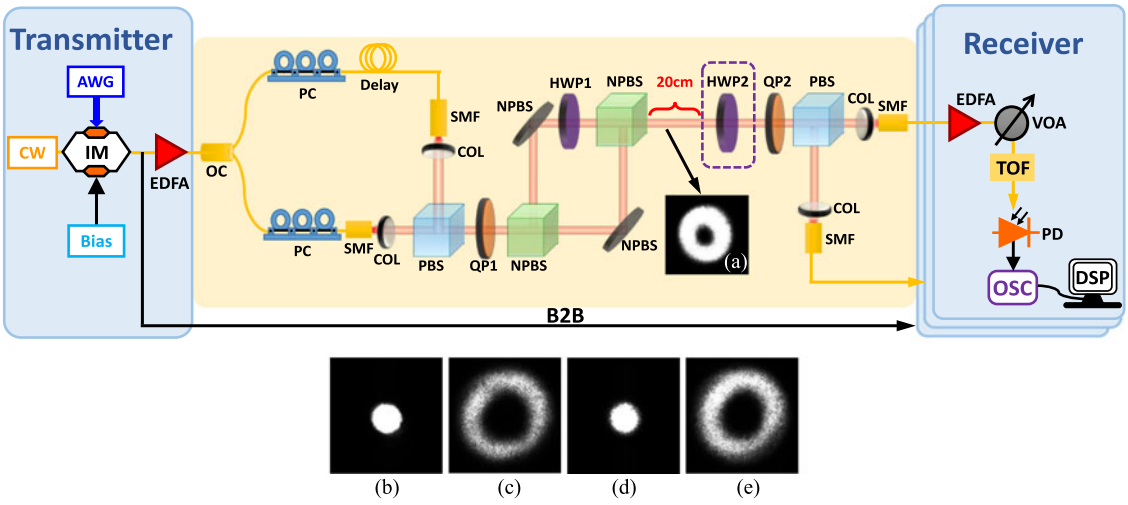

Fig. 4. The experimental setup of VMDM transmission system. CW: continuous wave; IM: intensity modulator; AWG: arbitrary waveform generator; EDFA: erbium-doped fiber amplifier; OC: optical coupler; PC: polarization controller; SMF: single mode fiber; COL: collimator; PBS: polarization beam splitter; QP: Q-plate; NPBS: non-polarizing beam splitter; HWP: half-wave plate; VOA: variable optical attenuator; TOF: tunable optical filter; PD: photo-detector; OSC: oscilloscope; DSP: digital signal processing. Recorded intensity patterns of (a) the four multiplexed VMs, (b) the demultiplexed HE_{21}^{even} and HE_{21}^{odd} channels, (c) the un-demultiplexed TE_{01} and TM_{01} channels, (d) the demultiplexed VMs corresponding to TE_{01} and TM_{01} channels, (e) the un-demultiplexed HE_{21}^{even} and HE_{21}^{odd} channels.

the SOPs of the corresponding four CVBs. By rotating the linear polarizer placed in front of CCD camera to a particular angle, the captured intensity profiles can be used to characterize the SOP of CVBs. Hence, the higher-order VMs can be effectively generated based on the simple setup.

After demonstration of the theoretical analysis and experimental verification of mode conversion, then we apply the generated CV modes, TE01, TM01, $HE_{21}^{even}/HE_{21}^{odd}$ modes, to demonstrate the CVB-based VMDM FSO transmission with high-speed data rate.

3.2. VMDM-DD-OFDM FSO Transmission Experiment

The experimental setup of CVB-based VMDM-DD-OFDM transmission system over free space optical (FSO) link for short reach optical interconnect is shown in Fig. 4. The center wavelength of external cavity laser (ECL) at transmitter is tuned to1550 nm. The lightwave is launched to an intensity modulator (IM, PhotolineMX-LN-40) which is modulated by a quadrature phase shift keying (QPSK)-OFDM signal generated by an arbitrary waveform generator (AWG, Tektronix AWG 70002A) with a 25Gs/s sampling rate. The IFFT size for QPSK-OFDM signal generation is 512, of which 246 low positive frequency subcarriers carry data and another 246 low negative frequency subcarriers are set as the complex conjugate of the positive frequency subcarriers to generate real-value OFDM signal. The 1st subcarrier of the FFT array is set to zero for DC-bias. The rest

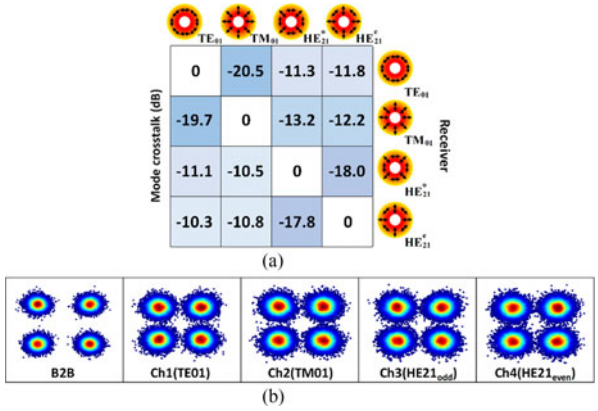

Fig. 5. (a) Normalized mode crosstalk matrix for four channels. (b) Constellations for B2B, Ch1, Ch2, Ch3, Ch4 when the received optical power is –20 dBm.

19 high frequency subcarriers are also set zeros for oversampling. A 32-sample cyclic prefix (CP) is added to the 512 samples, giving 544 samples per OFDM symbol. One training sequence is added in the front of 100 OFDM signal symbols to realize time synchronization and channel estimation. After amplified by a low noise erbium-doped fiber amplifier (EDFA), the optical signal is divided into two branches with an optical coupler (OC). Two polarization controllers (PCs) are used to maximize output power of horizontal and vertical polarization light from polarization beam splitter (PBS). The linear combination of horizontal and vertical polarization light is converted to TE01 mode and TM01 mode after passing through QP1. Then, the light beams are separated by a non-polarizing 50:50 beam splitters (NPBS). One branch is switched into $HE_{21}^{even}/HE_{21}^{odd}$ by means of HWP ($\alpha = \pi/2$). Subsequently, two branches including four VMs are combined by the second NPBS. The raw bit rate on each vector mode is 23.79 Gb/s ($25 \times 246/512 \times 100/101 \times 2\,\text{Gb/s} \asymp 23.79\,\text{Gb/s}$) which makes the aggregate raw bit rate of this demonstration be $4 \times 23.79\,\text{Gb/s} = 95.16$ Gb/s. Inset (a) in Fig. 4 shows the intensity pattern corresponding to the four multiplexed CVBs.

At receiver, mode demultiplexing is implemented by dividing the optical signals into two parts after transmitted over ~20 cm free space. When we place the HWP2 ($\alpha = \pi/2$) in the optical path (dotted-rectangle in Fig. 4), $HE_{21}^{even}/HE_{21}^{odd}$ are transformed back into the fundamental mode after propagating through the HWP2 and QP2. Fig. 4(b) shows the intensity pattern of the demultiplexed VMs corresponding to $HE_{21}^{even}/HE_{21}^{odd}$ channels. Meanwhile, TE_{01} and TM_{01} modes are transferred to higher-order VMs which cannot be coupled into single mode fiber (SMF). Fig. 4(c) shows the intensity pattern of the un-demultiplexed higher-order VMs corresponding to TE_{01} and TM_{01} channels. When we remove this HWP2 (dotted-rectangle in Fig. 4), only TE_{01} and TM_{01} modes are demodulated. The intensity pattern of the demultiplexed VMs and the un-demultiplexed higher-order VMs are depicted in insets 4(d) and 4(e), respectively. We can then use PBS to split two orthogonal SOPs of the demodulated beams. In this way, four VM channels can be successfully separated.

Meanwhile, the optical signals at the receiver are first amplified by another EDFA and then attenuated by a variable optical attenuator (VOA). After being filtered by a 1-nm bandwidth tunable optical filter (TOF) and received by a photo-detector (PD, u2t XPDV2120R), the signal is demodulated using real-time oscilloscope (OSC, Tektronix DSA 72004B) with 50GSa/s sample rate and further processed for the off-line digital signal processing (DSP). The digital signal processing algorithms include CP removal, FFT, channel estimation with Intra-symbol frequency-domain averaging (ISFA) [34], one-tap equalization, QPSK de-mapping and error counting. In the period of calibration, pre-equalization is implemented to overcome serious intra-symbol interference (ISI) induced by the high frequency power attenuation [35]. Fig. 5(a) shows the measured mode crosstalk of the four VMs in this experiment. The modal isolation (MI) is employed to define the modal crosstalk when the four VMs are transmitted simultaneously. The maximum MI is around -10.3 dB between different mode channels. The cause for crosstalk is due to mode conversion efficiency of QPs and the interference

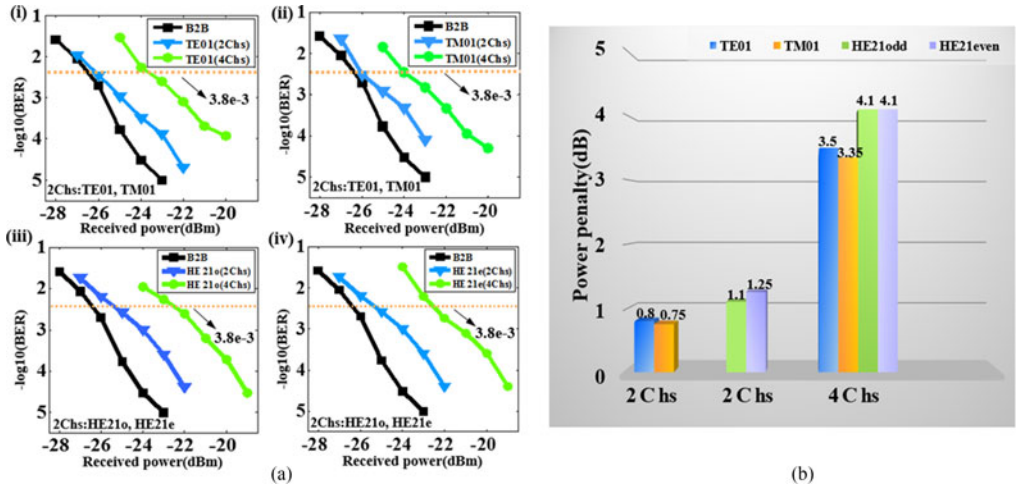

Fig. 6. (a) BER performance of TE01, TM01, HE_{21}^{even} and HE_{21}^{odd} channel for the two cases corresponding to two channels (2 Chs) and four channels (4 Chs) transmitted, respectively. B2B: back to back. (b) The power penalties for the VM channels corresponding to Fig. 6(a).

between VMs. Fig. 5(b) shows the constellations in the cases of "back to back" (B2B) transmission and four VM channels when the received power is equivalent to −20 dBm. As we can see, there are only slight differences of the constellations of these VMs channels.

To further investigate the transmission performance of VM channels, we measure and compare the BER property versus the received optical power when two CVB channels and four CVB channels are utilized to transmit signal. The measured experimental results are shown in Fig. 6(a). When the two channels of TE_{01} and TM_{01}, or $HE_{21}^{even}/HE_{21}^{odd}$ are transmitted, 0.8 dB and 0.75 dB, or 1.1 dB and 1.25 dB power penalties are induced between the B2B and CVB channels respectively under the forward error correction (FEC) threshold of 3.8×10^{-3}. We can find that the selected two channels differ slightly. When four channels are transmitted simultaneously, the error-free transmission for each VM channel can be realized with increased power penalties. There are 3.5 dB, 3.35 dB, 4.1 dB and 4.1 dB power penalties for TE_{01}, TM_{01}, $HE_{21}^{even}/HE_{21}^{odd}$ CVB channels, respectively. We can also find from Fig. 6(b) that the penalty difference between TE_{01} and TM_{01} (0.05 dB and 0.15 dB respectively), and that between $HE_{21}^{even}/HE_{21}^{odd}$ (0.05 dB and 0 dB respectively) remains small, for both the two-channel and the four-channel transmission. In addition, the performance of TE_{01} and TM_{01} channels are always better than $HE_{21}^{even}/HE_{21}^{odd}$ channels, and this result may be induced by the larger mode crosstalk.

It should be noted some factors that will influence the transmission distance of this proposed CVB-based VMDM system. First, the distance over FSO link is always limited by optical diffraction. The divergence of donut-shaped vector modes due to beam diffraction will be faster than that of the fundamental mode. Then the size of diverged vector modes will become larger than that of the receiver-end aperture after long transmission distance in FSO [36], [37]. This will significantly limit the transmission distance. Second, the characteristic of vector modes is also an important factor since it decides the Rayleigh range, and only within this transmission range the system performance can keep good [37], [38]. Third, the larger mode crosstalk of multiple vector modes further shortens the transmission distance. In the end, atmospheric turbulence as well as light wavelength will also have influence on transmission distance of CVB-based VMDM system. However, the impact of these factors can be decreased if more advanced technologies are adopted [39].

4. Conclusion

We introduce high-order Poincaré sphere model to investigate the state of polarization conversion of vector mode. This scheme provides a simple and flexible method to realize conversion of arbitrary

vector mode. The validation of high efficient mode conversion based on Q-plate and conventional half-waveplate is implemented and has good agreement with the theoretical analysis. Then, we apply this vector mode conversion to demonstrate 95.16 Gb/s 4-CVB-based VMDM transmission system.

References

[1] D. Ckilper, K. Bergman, V. Schan, I. Monga, G. Porter, and K. Rauschenbach, "Optical networks come of age," *Opt. Photon. News*, vol. 25, no. 9, pp. 50–57, 2014.
[2] IEEE P802.3bs 400 Gb/s Ethernet Task Force. (2015). [Online]. Available: http://www.ieee802.org/3/bm/index.html
[3] L. Luo *et al.*, "WDM-compatible mode-division multiplexing on a silicon chip," *Nat. Commun.*, vol. 5, 2015, Art. no. 3069.
[4] D. Richardson, J. Fini, and L. Nelson, "Space-division multiplexing in optical fibres," *Nat. Photon.*, vol. 7, no. 5, pp. 354–362, 2013.
[5] P. Winzer, "Spatial multiplexing in fiber optics: The 10× scaling of metro/core capacities," *Bell Labs Tech. J.*, vol. 19, pp. 22–30, 2014.
[6] G. Li, N. Bai, N. Zhao, and C. Xia, "Space-division multiplexing: The next frontier in optical communication," *Adv. Opt. Photon.*, vol. 6, no. 4, pp. 413–487, 2014.
[7] H. Wen *et al.*, "First demonstration of six-mode PON achieving a record gain of 4 dB in upstream transmission loss budget," *J. Lightw. Technol.*, vol. 34, no. 8, pp. 1990–1996, Apr. 2016.
[8] J. Luo, J. Li, Q. Sui, Z. Li, and C. Lu, "40 Gb/s mode-division multiplexed DD-OFDM transmission over standard multi-mode fiber," *IEEE Photon. J.*, vol. 8, no. 3, Jun. 2016, Art. no. 7905207.
[9] J. Wang *et al.*, "Terabit free-space data transmission employing orbital angular momentum multiplexing," *Nat. Photon.*, vol. 6, no. 7, pp. 488–496, 2012.
[10] A. Willner *et al.*, "Optical communications using orbital angular momentum beams," *Adv. Opt. Photon.*, vol. 7, no. 1, pp. 66–106, 2015.
[11] T. Lei *et al.*, "Massive individual orbital angular momentum channels for multiplexing enabled by Dammann gratings," *Light-Sci. Appl.*, vol. 4, 2015, Art. no. e257.
[12] J. Wang, "Data information transfer using complex optical fields: A review and perspective," *Chin. Opt. Lett.*, vol. 15, no. 3, 2017, Art. no. 030005.
[13] S. Chen *et al.*, "Full-duplex bidirectional data transmission link using twisted lights multiplexing over 1.1-km orbital angular momentum fiber," *Sci. Rep.*, vol. 6, 2016, Art. no. 38181.
[14] G. Xie *et al.*, "Experimental demonstration of a 200-Gbit/s free-space optical link by multiplexing Laguerre–Gaussian beams with different radial indices," *Opt. Lett.*, vol. 41, no. 15, pp. 3447–3450, 2016.
[15] L. Zhu and J. Wang, "Demonstration of obstruction-free data-carrying N-fold bessel modes multicasting from a single gaussian mode," *Opt. Lett.*, vol. 40, no. 23, pp. 5463–5466, 2015.
[16] G. Milione, T. A. Nguyen, J. Leach, D. A. Nolan, and R. R. Alfano, "Using the nonseparability of vector beams to encode information for optical communication," *Opt. Lett.*, 40, pp. 4887–4890, 2015.
[17] G. Milione *et al.*, "4 × 20 Gbit/s mode division multiplexing over free space using vector modes and a q-plate mode (de)multiplexer," *Opt. Lett.*, vol. 40, no. 9, pp. 1980–1983, 2015.
[18] Y. Zhao and J. Wang, "High-base vector beam encoding/decoding for visible-light communications," *Opt. Lett.*, vol. 40, no. 21, pp. 4843–4846, 2015.
[19] J. Zhang, F. Li, J. Li, Y. Feng, and Z. Li, "120 Gbit/s 2 × 2 vector-modes-division-multiplexing DD-OFDM-32QAM free-space transmission," *IEEE Photon. J.*, vol. 8, no. 6, Dec. 2016, Art. no. 7907008.
[20] Q. Zhan, "Cylindrical vector beams: From mathematical concepts to applications," *Adv. Opt. Photon.*, vol. 1, no. 1, pp. 1–57, 2009.
[21] S. Ramachandran, P. Kristensen, and M. Yan, "Generation and propagation of radially polarized beams in optical fibers." *Opt. Lett.*, vol. 34, no. 16, pp. 2525–2527, 2009.
[22] W. Cheng, J. W. Haus, and Q. Zhan, "Propagation of vector vortex beams through a turbulent atmosphere," *Opt. Exp.*,, vol. 17, no. 20, pp. 17829–17836, 2009.
[23] D. Naidoo *et al.*, "Controlled generation of higher-order Poincaré sphere beams from a laser," *Nat. Photon.*, vol. 10, pp. 327–332, 2016.
[24] S. Slussarenko, A. Murauski, T. Du, V. Chigrinov, L. Marrucci, and E. Santamato, "Tunable liquid crystal q-plates with arbitrary topological charge," *Opt. Exp.*,, vol. 19, no. 5, pp. 4085–4090, 2011.
[25] P. Chen, W. Ji, B. Wei, W. Hu, V. Chigrinov, and Y. Lu, "Generation of arbitrary vector beams with liquid crystal polarization converters and vector-photoaligned q-plates," *Appl. Phys. Lett.*, vol. 107, no. 24, 2015, Art. no. 241102.
[26] X. Yi *et al.*, "Generation of cylindrical vector vortex beams by two cascaded metasurfaces," *Opt. Exp.*,, vol. 22, no. 14, pp. 17207–17215, 2014.
[27] H. Huang *et al.*, "Mode division multiplexing using an orbital angular momentum mode sorter and MIMO DSP over a graded-index few mode optical fibre," *Sci. Rep.*, vol. 5, 2015, Art. no. 14931.
[28] X. Weng, L. Du, A. Yang, C. Min, and X. Yuan, "Generating arbitrary order cylindrical vector beams with inherent transform mechanism," *IEEE Photon. J.*, vol. 9, no. 1, Feb. 2017, Art. no. 6100208.
[29] Z. Liu *et al.*, "Generation of arbitrary vector vortex beams on hybrid-order Poincaré sphere," *Photon. Res.*, vol. 5, no. 1, pp. 15–21, 2017.
[30] M. Stalder and M. Schadt, "Linearly polarized light with axial symmetry generated by liquid-crystal polarization converters," *Opt. Lett.*, vol. 21, no. 23, pp. 1948–1949, 1996.
[31] G. Milione, S. Evans, D. Nolan, and R. Alfano, "Higher order pancharatnam-berry phase and the angular momentum of light," *Phys. Rev. Lett.*, vol. 108, no. 19, 2012, Art. no. 190401.

[32] L. Marrucci, C. Manzo, and D. Paparo, "Optical spin-to-orbital angular momentum conversion in inhomogeneous anisotropic media," *Phys. Rev. Lett.*, vol. 96, no. 16, 2006, Art. no. 163905.
[33] [Online]. Available: http://www.arcoptix.com/Q_Plate.htm?gclid = CLCZzeysjM4CFdiKaAodqqMLQA
[34] X. Liu and F. Buchali, "Intra-symbol frequency-domain averaging based channel estimation for coherent optical OFDM," *Opt. Exp.*,, vol. 16, no. 26, pp. 21944–21957, 2008.
[35] F. Li, X. Li, J. Zhang, and J. Yu, "Transmission of 100-Gb/s VSB DFT-spread DMT signal in short-reach optical communication systems," *IEEE Photon. J.*, vol. 7, no. 5, Oct. 2015, Art. no. 7904307.
[36] P. Greene and D. Hall, "Diffraction characteristics of the azimuthal bessel-gauss beam," *J. Opt. Soc. Amer. A*, vol. 13, no. 5, pp. 962–966, 1996.
[37] P. Greene and D. Hall, "Properties and diffraction of vector Bessel–Gauss beams," *J. Opt. Soc. Amer. A*, vol. 15, no. 12, pp. 3020–3027, 1998.
[38] O. Edfors and A. Johansson, "Is orbital angular momentum (oam) based radio communication an unexploited area?" *IEEE Trans. Antennas Propag.*, vol. 60, no. 2, pp. 1126–1131, Feb. 2012.
[39] Y. Ren *et al.*, "Adaptive-optics-based simultaneous pre- and post-turbulence compensation of multiple orbital-angular-momentum beams in a bidirectional free-space optical link," *Optica*, vol. 1, no. 6, pp. 376–382, 2014.